Journal of Materials Chemistry B

RSC Publishing

PAPER

View Article Online
View Journal

Influenza A virus molecularly imprinted polymers and their application in virus sub-type classification†

Cite this: DOI: 10.1039/c3tb00027c

Thipvaree Wangchareansak,[ac] Arunee Thitithanyanont,[b] Daungmanee Chuakheaw,[a] M. Paul Gleeson,[a] Peter A. Lieberzeit[c] and Chak Sangma*[a]

Received 8th January 2013
Accepted 18th February 2013

DOI: 10.1039/c3tb00027c

www.rsc.org/MaterialsB

In this work, we apply a molecular imprinting strategy as a screening protocol for different influenza A subtypes, namely H5N1, H5N3, H1N1, H1N3 and H6N1. Molecularly imprinted polymers for each of these subtypes lead to appreciable sensor characteristics on a quartz crystal microbalance leading to detection limits as low as 10^5 particles per ml. Selectivity studies indicate that each virus is preferably incorporated by its own MIP. Recognition in most cases is dominated by the neuraminidase residue rather than the hemagglutinin. Multivariate analysis shows that the sensor responses can be correlated with the differences in hemagglutinin and neuraminidase patterns from databases. This allows for virus subtype characterization and thus rapid screening.

Published on 19 February 2013 on http://pubs.rsc.org | doi:10.1039/C3TB00027C
Downloaded by Australian National University on 12 March 2013

Introduction

Only a limited number of cases have been reported where humans have suffered H5N1 infection.[1–5] However, there is a real risk that a highly pathogenic strain could cause a global pandemic if it develops the ability to more effectively jump species *via* selective mutation.[6–11] This is particularly true since it has been shown in the literature that simple mutations of the avian virus can lead to avian H5N1 strains more capable of infecting mammals.[12]

To face this threat, experiments on highly pathogenic strains of the H5N1 virus are needed, despite the obvious threat they pose.[13–15] However, there are substantial limitations in performing such experiments, since they must be carried out in a secure laboratory setting, which is time consuming and expensive. For instance, conventional morphology studies, or antibody affinity tests, rely on "live" viruses to obtain reliable data and have, therefore, to be performed under special safety regimes.[16,17] The determination of the influenza A virus subtypes, as well as physical characteristics, including shape, size or morphology is among the critically important fundamental experiments.[18–21] Cheaper, safer and more convenient methods to assess these aspects are therefore of obvious attraction.[22]

The molecular imprinting technique[23–28] is a very versatile method that has been used in diverse applications[29–32] including molecular sensing,[33] antibody screening,[34] drug delivery[35,36] and protein[27] and virus classification.[30,37,38] Molecularly Imprinted Polymer (MIP) can be created *via* polymerizing a highly cross-linked matrix in the presence of a template. This can consist of individual molecules or mixtures thereof, proteins or even larger species including viruses. The imprinting process therefore results in a "negative" image of the template being imprinted into the polymer itself. Removing the original template from the polymer reveals accessible cavities on its surface that retain selective molecular information regarding both morphological and functional properties of the template.[39] MIPs are both rapid and relatively inexpensive to produce and offer significant potential for use in a screening environment.[40] The unique shape selectivity defined by the original template leads to an MIP that can potentially allow us to differentiate between even subtly different molecular systems.[41,42]

A number of transducer principles can be applied to assess the extent of binding to an MIP, including quartz crystal microbalance (QCM),[43–45] surface plasmon resonance (SPR)[46,47] and electrochemical devices.[48–52] In this study we focus on QCM, a reliable technique that has been widely applied in chemo- and biosensors.[43–45,53,54] They rely on the intrinsic oscillation characteristics of quartz crystals, and the fact that there is a linear relationship between this frequency and the mass absorbed onto the crystal surface. Thus, for the quartz/MIP electrodes used in this study, the oscillation frequency changes depending on the extent of sample binding to the MIP. In principle, only the original template is expected to give rise to the same frequency found for the MIP/quartz system before template removal. Additionally, species that do not bind, whatsoever, to the MIPs should not lead to measurable sensor signals. The

[a]Department of Chemistry, Faculty of Science, Kasetsart University, Chatuchak, Bangkok, Thailand. E-mail: fscicsm@ku.ac.th; Fax: +66-2-5793955; Tel: +66-2-562-5555 ext. 2192

[b]Department of Microbiology, Faculty of Science, Mahidol University, Rama 6 road, Payatai, Bangkok, Thailand

[c]University of Vienna, Department of Analytical Chemistry, Vienna, Austria

† Electronic supplementary information (ESI) available: An expanded description of the experimental methods used in this study, along with tables showing the sequence similarity and MIP results for each virus. See DOI: 10.1039/c3tb00027c

Published on 19 February 2013 on http://pubs.rsc.org | doi:10.1039/C3TB00027C
Downloaded by Australian National University on 12 March 2013

frequency changes between successive binding experiments according to the Sauerbrey equation.[55]

$$\Delta f = -c\Delta m \quad (1)$$

where Δf represents the frequency change depending on mass loading, Δm refers to mass loading on a QCM. The sensitivity of the QCM to the addition of mass, c, can therefore be calculated to be approximately 4.6 Hz per ng of molecule binding in the gas phase for a device having a resonance frequency of $f_0 = 10$ MHz. In fact, Sauerbrey equation is only valid in the gas phase. For the use in the liquid state, the influence of viscosity and density of the surrounding liquid has to be considered as described by Kanazawa and Gordon.[56] In our experiment, this nonspecific influence is compensated by using a dual-electrode setup. The signal difference between the two electrodes comes only from the absorbed mass on the working electrode. Contributions to the signal from other sources will be comparable on the reference and the working electrode and so will cancel out.

In this work, we combine MIPs and QCM for the proof-of-concept of a screening protocol for influenza A. To the best of our knowledge, this is the first study reporting the successful creation of influenza A based MIPs. Five relatively common virus strains (H5N1, H5N3, H1N1, H1N3 and H6N1) have been used to create five unique MIPs. The relative selectivity of the five different influenza A viruses for each of the five MIPs is then assessed to ascertain whether such a method is sufficiently selective to allow for discrimination between the different virus sub-types. The value of such a method is that it could be quickly and cheaply employed to characterize the identity of unknown influenza A virus samples, or updated with new viruses as they became known.

Materials and methods

Avian influenza H5N1 and H6N1 viruses were isolated from an open-billed stork and duck, respectively. The original stock of reassortant vaccine virus A/California/7/2009 (H1N1)-like strain was obtained from WHO Collaborating Centre in CDC, USA. Reverse genetic H1N3 and H5N3 viruses were obtained from the National Center for Genetic Engineering and Biotechnology, Thailand. All viruses were propagated in MDCK cells according to the standard WHO protocol[57] and inactivated with β-propiolactone following a modified CDC protocol (see ESI†) at the Department of Microbiology, Mahidol University, Bangkok, which has access to P3 biosafety laboratories. The inactivated viruses were investigated for HA titer using a hemagglutination assay and for viral infectivity by passaging in MDCK cells for 6 days.[58]

Molecular imprinting

The overall strategy for assembling the biosensors used in this work is shown in Fig. 1: co-polymers used in the MIP production consisted of 13.0 mg of acrylamide (AMM, purchased from Acros), 10.6 mg of methacrylic acid (MAA, purchased from Sigma-Aldrich), 6 mg of methylmethacrylate (MMA, purchased from Sigma-Aldrich) and 6.3 mg of *N*-vinylpyrrolidone (VP, purchased from Sigma-Aldrich) as monomers, mixed with 48 mg of the cross-linker *N*,*N*-(1,2-dihydroxyethylene) bisacrylamide (DHEBA, obtained from Alfa Aesar). This mixture was dissolved in 300 μl of dimethylsulfoxide (DMSO, obtained from Merck in analytical grade) containing 1 mg of 2,2′-azobis(isobutyronitrile) (AIBN, purchased from Sigma-Aldrich) as initiator. Afterwards, this was followed by pre-polymerization at 70 °C just prior to reaching the gel point in approximately 40 minutes. A template stamp was prepared by dropping 5 μl of influenza virus on a bare glass plate which was maintained at 4 °C for 30 minutes to allow for sedimentation and to avoid interference from the buffer media in the MIP creation process. After this, excess buffer was spun off at 3000 rpm. In parallel, the polymer was spin-coated onto both QCM electrodes at 3000 rpm to obtain thin layers of 350 to 450 nm thickness. Previous studies[59] showed that bioimprinting takes place strictly on the surface of the respective polymer, which makes controlling the layer height down to one nanometer unnecessary. Immediately, the stamp coated with the template virus was pressed onto the spin-coated pre-polymer and polymerized under 254 nm UV light overnight. Finally, the template was removed from the polymer surface by rinsing it with 10% hydrochloric acid to denature the virus and then stirred in water at 45 °C for 3 hours to remove the virus particles left on the surface. This resulted in cavities on the rigid polymer surface that were ready to be applied on the QCM as biosensor.

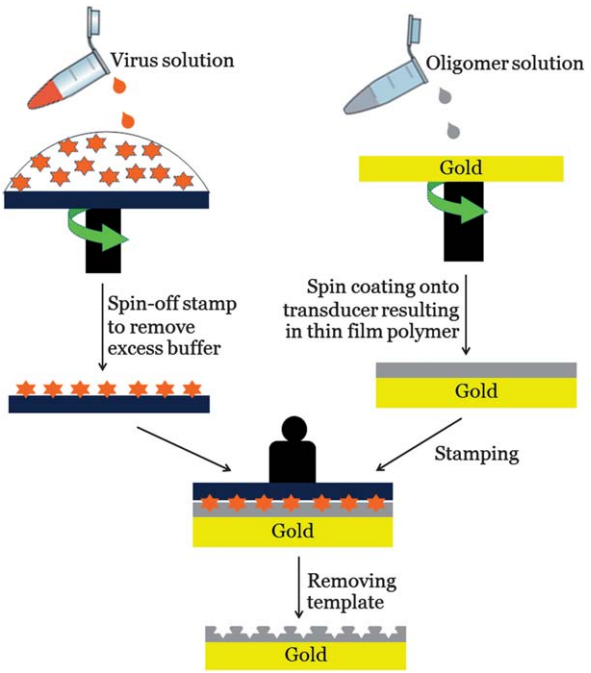

Fig. 1 Schematic of the imprinting protocol used.

QCM preparation and measurement

Dual gold electrodes were generated on an AT-cut quartz wafer, 15.5 mm in diameter and 168 μm in thickness with screen-printing, using a procedure as described in previous work.[60] The electrode diameter on the sample side was 5 mm and 4 mm on

This journal is © The Royal Society of Chemistry 2013

Published on 19 February 2013 on http://pubs.rsc.org | doi:10.1039/C3TB00027C
Downloaded by Australian National University on 12 March 2013

the other side (see ESI†). The QCM electrodes were connected to a home-built oscillator circuit read out by a frequency counter (Agilent 53131A). Measurement data were transferred to a PC *via* a GPIB USB interface *via* a custom-made LabView routine. All measurements were carried out in stop-flow mode at room temperature and were made in triplicate for the two separate MIPs produced for each virus type.

Characterization

The MIPs were verified by a Veeco Nanoscope IVa Atomic force microscope (AFM). All AFM images were operated in contact mode using a Veeco SNL-10 silicon tip with a spring constant of 40 Nm and onset pressure corresponding to differential signal 1 V on a photodiode.

Results and discussion

Synthesis and structural characterization of MIPs

MIPs were prepared using the polymerization protocol adapted from our previous work on glycoproteins.[61] The rationale behind this is that approximately 80% of the influenza virus surface is made up of the glycoproteins hemagglutinin (HA) and neuraminidase (NA). Initial co-polymers consisted of AAM, MAA, MMA and VP as monomers. However, the resulting MIPs were not capable of differentiating between the 5 different virus sub-types. This led to the modification of that monomer system by including VP as an additional monomer resulting in a dramatic increase in the selectivity displayed by the MIP for the influenza A virus sub-types. The sensitivity and selectivity of the method was further refined by adjusting the ratio between the different monomers and the cross-linker.

However, the first step in the imprinting experiments, of course, consisted of verifying the imprinting process using AFM. Fig. 2 shows the AFM images of a representative MIP (H1N3) produced in this study: images were recorded for the virus templates (Fig. 2a), the imprinted MIP/virus following polymerization (Fig. 2b) and a blank, and non-imprinted polymer (NIP) formed without a template (Fig. 2c). Finally, in Fig. 2d, an image of a MIP having been exposed to a H1N3 suspension after template removal is shown. Obviously, the layer has re-incorporated virus particles from its environment, as marked by red circles.

The size distribution of the influenza A virus shown in Fig. 2a was found to be between 80 and 120 nm, which corresponds well to the values found in the literature.[62–64] This is also comparable to the diameters of the pores found on the MIPs illustrated in Fig. 2b, further suggesting that the MIP generation process was successful. The ability of the bare MIPs (Fig. 2c) to re-bind the influenza A virus following the template removal was also confirmed based on the AFM image in Fig. 2d. Fig. 2d shows a much larger number of white spots of ~100 nm in diameter, which is indicative of bound virus.

Influenza-A sensitivity of MIPs

Following confirmation of the successful imprinting procedure, each of the five MIPs was coated onto the gold electrodes of a dual-electrode QCM. To act as a reference, one channel contained a non-imprinted polymer (NIP) so as to assess the influence of the surrounding environment (*i.e.* pH, temperature and nonspecific polymer–virus interactions), while the second contained the influenza virus derived MIP.

Fig. 3 shows a standard response curve for a QCM MIP experiment over time, and the linear relationship between the logarithm of virus concentrations and frequency (r^2 = 0.98)

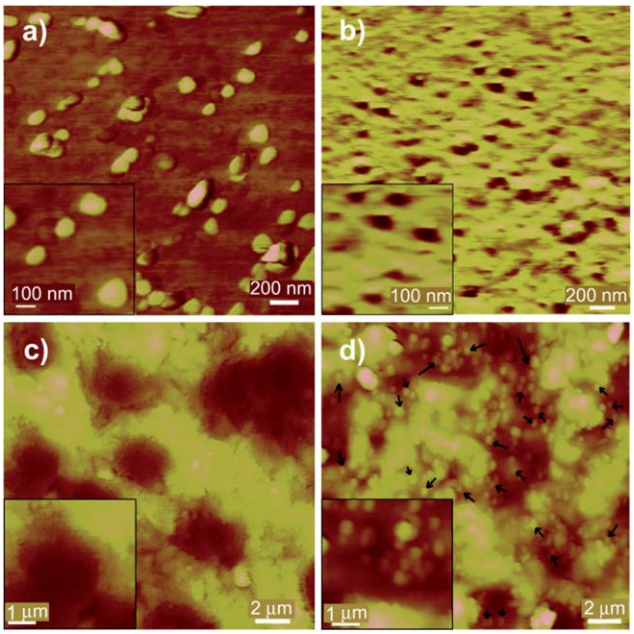

Fig. 2 AFM images of (a) the H1N3 influenza A virus used as a template, (b) the corresponding H1N3 based MIPs at 200 nm resolution. The MIP cavities in the latter have been found to be between 80 and 120 nm in diameter, which is the expected size of influenza A.[62–64] Also illustrated is the structure of the MIP with (c) and without template bound (d) displayed at 2 µm resolution. The white spots present in the template bound structure (d) are indicative of bound virus (some bound virus is marked by dark arrows).

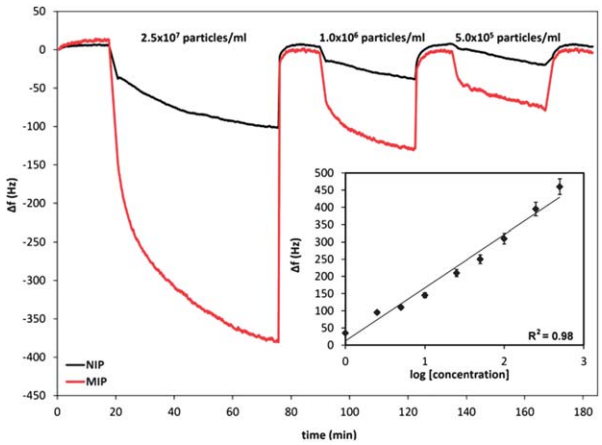

Fig. 3 A typical outcome of an MIP QCM experiment. Also shown for comparison is the response of a non-imprinting polymer (NIP). The initial baseline signal of the unoccupied MIP is recorded in buffer solution. Absorption to the MIP is characterized by a drop in frequency on exposure to virus solution. In the inset, the effect of virus concentration with frequency is given (r^2 = 0.98).

Published on 19 February 2013 on http://pubs.rsc.org | doi:10.1039/C3TB00027C
Downloaded by Australian National University on 12 March 2013

(Fig. 3, inset). The sensor signal in Fig. 3 still shows some drift in both channels but the difference between the MIP channel and the reference remains constant after about 20 minutes following sample injection at the lower sample concentrations. A fully horizontal response was only achieved after 3–4 h due to slow sedimentation of the virus, thus a time point of 40 minutes following injection was used as the standard. A logarithmic relationship can be expected with sensor measurements including samples covering several orders of magnitude of concentration due to saturation effects on the polymer surface. This, of course, does by no means contradict our previous statement that a QCM generally responds to mass changes in a linear way. One can see that at any given time the MIP signal substantially exceeds that of the NIP, providing further corroborating evidence for the success of the imprinting approach. On reaching equilibrium between the MIP layer and surrounding sample solution, the ratio of the MIP/NIP signals is at least five-fold. Although it would of course be desirable to have no unspecific effects on the NIP at all, this in reality cannot be achieved. This is also corroborated by recent studies showing that good-quality MIPs usually consist of polymers that also have some non-specific interaction with the respective template.[65] For each experiment, the MIP/NIP dual electrode system is first immersed in phosphate buffer PBS (1 mM, pH 7.2) until constant reading is reached. The PBS solution is then removed from the measuring chamber containing both samples and is flushed with 75 μl of virus sample. The chamber is then completely filled with the virus sample and monitored until a constant QCM signal is obtained. Before the MIP can be reused to assess a new virus solution, the previous virus solution is washed out from the chamber seven times, once with 10% of acetic acid, four times with water and two times with PBS solution. Only after the QCM signal has returned to its original baseline, a new experiment is started. Furthermore, measurements show that the noise level of the QCM sensors immersed in the virus samples is typically around 5 Hz. At 5×10^5 particles per ml the sensor response is 75 Hz leading to a limit of detection of 10^5 particles per ml following the IUPAC standards. Even though this does not reach the sensitivity levels obtained by modern PCR techniques due to the absence of amplification steps, it shows the very high potential of such MIPs for screening and rapid testing purposes once the concept has been proven (which is the aim of the current paper).

Influenza-A selectivity of MIPs

The use of MIPs to rapidly assess the identity of an unknown influenza A virus strain would be highly desirable. To obtain the proof of concept of such a method we have therefore undertaken sensor studies with a set of five common influenza A virus strains: H5N1, H1N1, H1N3, H6N1 and H5N3 MIPs were created for each virus strain. Each of the 5 virus strain MIPs was then exposed to all five solutions containing one virus subtype each. Within these experiments we used solutions containing 2×10^7 particles per ml. In all cases (Fig. 4), the virus sub-type used to create the MIP yielded the highest relative frequency change. This frequency shift is then used as the reference for all other

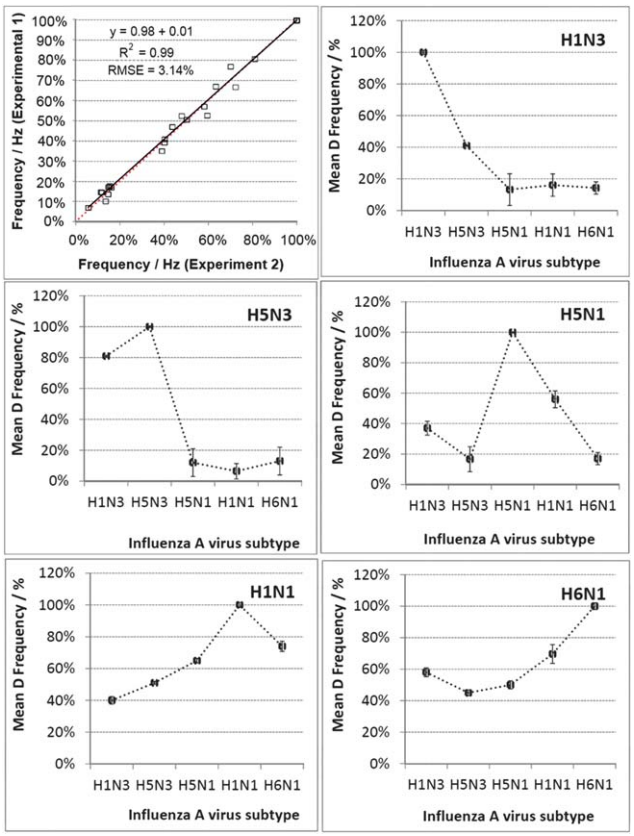

Fig. 4 Selectivity pattern of different influenza strain MIPs. Note that the highest signal for each MIP was always the signal from the virus used as the template and the nearest neighbours were those sharing the NA type.

virus subtypes and assigned a value of 100%. A value of 0% indicates that no frequency change can be observed. Fig. 4a shows a reproducibility study undertaken with two MIPs with the same template in five virus strains. Those MIPs were exposed to all virus types. Analysis of the results shows that they are highly reproducible ($r^2 = 0.99$), further supporting the power of these systems for screening purposes: The standard error was found to be 3.1% for the 50 different experiments. We therefore report the 95% confidence intervals (SE*2) in Fig. 4b–f.

The selectivity results obtained at virus concentrations of particles per ml displayed in Fig. 4b–f show that the virus used as a template to create the MIP in any case shows 100% response. No other virus reaches such a value for any given MIP. This is also true the other way round: no MIP yields higher sensor response for any given virus than towards its own template. For example, H1N3 leads to a sensor effect of 100% for its own MIP, while for the MIP belonging to the structurally related virus, H5N3, it displays a frequency change of ~80%. This value is well outside the 95% confidence intervals of the experimental method allowing us to definitively identify H1N3. For MIP templates with H5N1, H6N1 and H1N1, respectively, much smaller frequency changes of between 40 and 50% are observed. This result indicates that H1N3 can bind reasonably strongly to all MIPs produced here, but more strongly to MIPs based on a template sharing the same neuraminidase (NA) domain, namely N3. In contrast to H1N3, the H5N3 virus shows

 This journal is © The Royal Society of Chemistry 2013

Published on 19 February 2013 on http://pubs.rsc.org | doi:10.1039/C3TB00027C
Downloaded by Australian National University on 12 March 2013

much lesser affinity to MIPs imprinted with viruses containing the N3 domain. H5N3 shows a 100% frequency change for its own MIP, but <50% response across all other MIPs, including H1N3. This suggests that the hemagglutinin domain (HA) more substantially contributes to selectivity in this case. On the other hand, H5N1 virus particles have been found to bind more strongly to the MIP template with species containing the N1 domain, with negligible binding (<20%) for those of the N3 domain. H1N1 and H6N1 display very similar sensor responses on the different polymers, differing substantially only at their own respective MIPs. In these cases however, we see that both viruses do not bind strongly to either H5N1- or H1N3-based MIP suggesting that in this case both the H and the N domains are critical in governing recognition.

It can also be seen that each virus sample shows a strikingly different profile over the 5 different MIPs, in essence corresponding to a unique bio-molecular fingerprint. Thus both the response% compared to the standard and the overall profile across multiple MIPs could be used to definitively identify an unknown virus. For determining the constituents of a virus mixture, a single sensor of course is not sufficient. However, combining these MIPs in a sensor array, in conjunction with multivariate statistical analysis might prove useful. This would then also allow for quantifying viruses more accurately, because a single sensor could naturally only achieve this in the case where it was clear beforehand that a sample contains only one virus subtype. The value of the unique MIP fingerprint can be realized based on an analysis of the cross-screening results using principal components analysis (PCA). The inter-correlation between the response values obtained for the different virus samples for each MIP is graphically illustrated in the loading bi-plot shown in Fig. 5. In this plot, the descriptor loadings and the scores associated with the observations are displayed together to facilitate interpretation. The results for two MIPs with the same template are presented separately to help illustrate the sensitivity of the method. Briefly, the principal components consist of linear combinations of the original input variable, with each component being orthogonal to each other. On the loading bi-plot, descriptors and observations located close to each other on a given principal component are correlated (unless close to the origin). Descriptors or observations at the opposite ends of a particular component are inversely correlated.

The two-dimensional results displayed in Fig. 5 are a relatively simple way to represent the multiple measurements displayed in Fig. 4. Analysis of the correlation underlying the data (2 components describing 88.2% of the data) shows that the MIP results can lead to effective separation of the 5 different virus samples from one another. The information contained in component 1 describes 64.8% of the total variation in the dataset. It is found to primarily describe the separation between the group consisting of H6N1, H1N1 and H5N1 and that of H5N3 and H1N3. While component 1 also separates H5N3 and H1N3 to a degree, it is primarily related to the structural differences arising from the NA domain. This is consistent with the reports of Jin *et al.*,[66] who suggested that the type of the NA domain has a larger influence on the shape of influenza virus particles than HA.

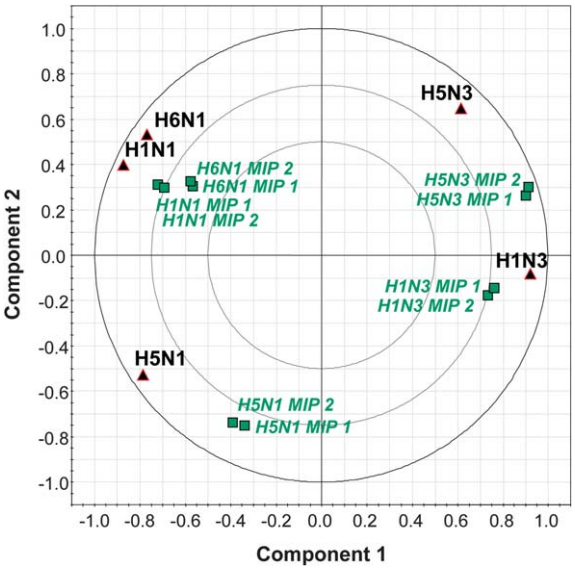

Fig. 5 Principal components analysis bi-plot showing the inter-relationship between the descriptors (green squares corresponding to the MIP measurements) and the influenza sub-type under investigation (black triangles). The PCA model fits 2 components, describing 88.2% of the total variation found in the 50 individual experiments (PC1 = 64.8% and PC2 = 23.4%). Note, clear separation between the sub-types can be seen. For H1N1 and H6N1 this can be done by an analysis of the absolute magnitude of the MIP input descriptors (*i.e.* correlation is the same, but larger values observed for H6N1).

Component 2 describes an additional 22% of the variation in the dataset. It allows us to separate both H5N1 and H1N3 from each other, and the group consisting of H1N1, H6N1 and H5N3. Separation between H1N1 and H6N1 is less effective using the 2

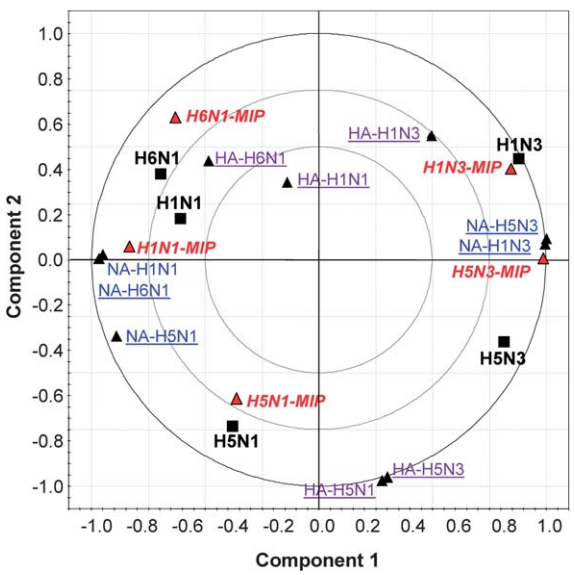

Fig. 6 Principal components analysis bi-plot showing the interrelationship between the MIP% change in response (red) and sequence similarity between the H (purple, underlined) and NA (blue, underlined) domains of the five different influenza-A sub-types. The influenza sub-types under investigation are denoted as green squares. The PCA model fits 2 components, describing 78.4% of the total variation (PC1 = 54.9% and PC2 = 23.6%).

Published on 19 February 2013 on http://pubs.rsc.org | doi:10.1039/C3TB00027C
Downloaded by Australian National University on 12 March 2013

components from PCA. This is simply because that the two viruses display a highly correlated response for all the MIPs investigated here, as already shown in the discussion of Fig. 4e and f. The key to differentiating between these viruses is their relative response over each other's MIP. It is also worth noting that the PCA results clearly show that H5N1 and H5N3 are essentially inversely correlated (found at extreme ends on both axes in Fig. 5). This suggests that the selectivity of a given MIP is not simply an additive effect due to its respective NA and HA domains.

To try and illustrate the link between the experimental MIP selectivity and the structural similarity between the NA and HA domains, we further analyzed a combined dataset containing the MIP selectivity data and the HA and NA sequence similarity data as obtained from nucleotide sequence (Fig. 6). The PCA results showed that there was a strong correlation between the MIP responses: The two-component model shows essentially the same separation as seen in Fig. 5. It also shows that the NA based similarity descriptors dominate component 1 and the HA based similarity descriptors dominate component 2.

MIP-based virus identification assays

The proof-of-concept results presented here clearly indicate that a useful screening protocol can be developed for influenza-A using an MIP based method. Furthermore, the results suggest that we do not necessarily need to produce MIPs for all possible influenza A sub-types. It appears that the use of a subset of MIPs would allow researchers to quickly categorize the respective virus sub-type as long as it is a combination of the already known HA and NA domains. For example, let us consider the use of just two of the MIPs for screening the five viruses under investigation here. An H1N3- and an H5N1-based MIP would allow us to selectively identify all 5 virus samples based on their frequency changes (Table 1). The use of measurements from an H1N3 based MIP would allow us to selectively separate H1N3 and H5N3 from the other N1 based virus samples (*i.e.* Δf measurements lying beyond the 95% confidence margins). Use of the H5N1 based MIP in conjunction with the H1N3 MIP would allow us to selectively identify H5N1, H1N1, and again H1N3. H6N1 can be differentiated from the others based on the fact that it displays Δf values below 20% in both MIPs, unlike any other virus sub-type.

Table 1 The average Δf/Hz values obtained for all 5 virus samples at two different MIPs. From these two results it is possible to selectively identify each virus sample. With the use of a much larger pool of MIP samples, a more selective bio-molecular fingerprint could be constructed to better identify the full range of influenza A viruses. * Indicates virus results that can be discriminated from others with greater than 95% confidence

Virus	H1N3 MIP	H1N1 MIP
H1N3	100%*	37%*
H5N3	41%*	17%
H5N1	13%	56%*
H1N1	16%	100%*
H6N1	14%	17%

Conclusions

Influenza H5N1 poses a considerable threat to the global population meaning that more rapid or reliable methods to screen for specific influenza types are desirable. In this work we assess the utility of an MIP technique for use in a screening protocol for influenza A. Five virus strains were used to design MIPs to facilitate easier handling of the proteins, and the rapid and accurate characterization of sub-types.

Our results show the feasibility of using influenza A virus MIPs as an alternative, rapid way to screen for sub-type selectivity in unknown samples. For all MIPs synthesized for this study, the virus sub-type used to create the MIP yielded the highest relative frequency change in the QCM experiment. It was also demonstrated that each virus sub-type showed a strikingly different profile over the 5 different MIPs, corresponding to a unique bio-molecular fingerprint. Thus both the response% compared to the standard, and the overall profile across multiple MIPs, could theoretically be used to definitively identify an unknown virus. Analysis of the experimental results using the multivariate PCA method shows that the origin of the different binding responses is primarily due to the NA domain, consistent with the reports of Jim *et al.*[66] However the selectivity of a given MIP is not simply an additive effect due to its respective NA and HA domains given that the Δf values of H5N3 and H5N1 are essentially inversely correlated.

Finally, the results presented here that a useful screening protocol could be developed for influenza-A using an MIP based method. Furthermore, the results suggest that we do not necessarily need to produce MIPs for all possible influenza A sub-type viruses to identify all sub-types. It appears that even using a small subset of MIPs could allow us to quickly categorize the sub-type. Further studies are now ongoing to assess the reliability of the method to further sub-types, as well as viruses expressed in different expression systems.

Acknowledgements

The authors thank the RGJ PhD program, Thailand Research Fund DBG5280004, ASEA-UNINET, Kasetsart National Research University Project, Kasetsart University Research and Development Institute for financial support of this work. We also thank S. Hannongbua, from Chulalongkorn University; S. Hannongbua and J. Limtrakul, from Kasetsart University, Thailand; and P. Wolschann, F.L. Dickert and F.M. Unger from the University of Vienna for their support of this study. We thank R. G. Webster and R. J. Webby for 8-plasmid reverse genetics system and N3 plasmid.

Notes and references

1 Q. M. Le, M. Kiso, K. Someya, Y. T. Sakai, T. H. Nguyen, K. H. L. Nguyen, N. D. Pham, H. H. Ngyen, S. Yamada, Y. Muramoto, T. Horimoto, A. Takada, H. Goto, T. Suzuki, Y. Suzuki and Y. Kawaoka, *Nature*, 2005, **437**, 1108.
2 J. J. Treanor, J. D. Campbell, K. M. Zangwill, T. Rowe and M. Wolff, *N. Engl. J. Med.*, 2006, **354**, 1343–1351.

 This journal is © The Royal Society of Chemistry 2013

Published on 19 February 2013 on http://pubs.rsc.org | doi:10.1039/C3TB00027C
Downloaded by Australian National University on 12 March 2013

3 G. Neumann, H. Chen, G. F. Gao, Y. L. Shu and Y. Kawaoka, *Cell Res.*, 2010, **20**, 51–61.
4 K. Das, J. M. Aramini, L. C. Ma, R. M. Krug and E. Arnold, *Nat. Struct. Mol. Biol.*, 2010, **17**, 530–538.
5 D. MacKenzie, in *New Scientist Magazine*, 2011, p. 14.
6 E. C. J. Claas, A. D. M. E. Osterhaus, R. van Beek, J. C. De Jong, G. F. Rimmelzwaan, D. A. Senne, S. Krauss, K. F. Shortridge and R. G. Webster, *Lancet*, 1998, **351**, 472–477.
7 B. Olsen, V. J. Munster, A. Wallensten, J. Waldenstrom, A. D. M. E. Osterhaus and R. A. M. Fouchier, *Science*, 2006, **312**, 384–388.
8 I. M. Longini, A. Nizam, S. F. Xu, K. Ungchusak, W. Hanshaoworakul, D. A. T. Cummings and M. E. Halloran, *Science*, 2005, **309**, 1083–1087.
9 J. K. Taubenberger and D. M. Morens, *Emerging Infect. Dis.*, 2006, **12**, 15–22.
10 J. K. Taubenberger and D. M. Morens, *Annu. Rev. Pathol.: Mech. Dis.*, 2008, **3**, 499–522.
11 K. Harmon, in *Scientific American* 2011.
12 S. Herfst, E. J. Schrauwen, M. Linster, S. Chutinimitkul, E. de Wit, V. J. Munster, E. M. Sorrell, T. M. Bestebroer, D. F. Burke, D. J. Smith, G. F. Rimmelzwaan, A. D. Osterhaus and R. A. Fouchier, *Science*, 2012, **336**, 1534–1541.
13 K. Y. Yuen, P. K. Chan, M. Peiris, D. N. Tsang, T. L. Que, K. F. Shortridge, P. T. Cheung, W. K. To, E. T. Ho, R. Sung and A. F. Cheng, *Lancet*, 1998, **351**, 467–471.
14 R. R. Regoes and S. Bonhoeffer, *Science*, 2006, **312**, 389–391.
15 D. J. Smith, *Science*, 2006, **312**, 392–394.
16 T. Rowe, R. A. Abernathy, J. Hu-Primmer, W. W. Thompson, X. H. Lu, W. Lim, K. Fukuda, N. J. Cox and J. M. Katz, *J. Clin. Microbiol.*, 1999, **37**, 937–943.
17 P. J. Collins, L. F. Haire, Y. P. Lin, J. F. Liu, R. J. Russell, P. A. Walker, J. J. Skehel, S. R. Martin, A. J. Hay and S. J. Gamblin, *Nature*, 2008, **453**, 1258–1261.
18 D. J. Jamieson, M. A. Honein, S. A. Rasmussen, J. L. Williams, D. L. Swerdlow, M. S. Biggerstaff, S. Lindstrom, J. K. Louie, C. M. Christ, S. R. Bohm, V. P. Fonseca, K. A. Ritger, D. J. Kuhles, P. Eggers, H. Bruce, H. A. Davidson, E. Lutterloh, M. L. Harris, C. Burke, N. Cocoros, L. Finelli, K. F. MacFarlane, B. Shu, S. J. Olsen and Novel Influenza A (H1N1) Pregnancy Working Group, *Lancet*, 2009, **374**, 451–458.
19 K. Hancock, V. Veguilla, X. H. Lu, W. M. Zhong, E. N. Butler, H. Sun, F. Liu, L. B. Dong, J. R. DeVos, P. M. Gargiullo, T. L. Brammer, N. J. Cox, T. M. Tumpey and J. M. Katz, *N. Engl. J. Med.*, 2009, **361**, 1945–1952.
20 J. Wrammert, D. Koutsonanos, G. M. Li, S. Edupuganti, J. H. Sui, M. Morrissey, M. McCausland, I. Skountzou, M. Hornig, W. I. Lipkin, A. Mehta, B. Razavi, C. Del Rio, N. Y. Zheng, J. H. Lee, M. Huang, Z. Ali, K. Kaur, S. Andrews, R. R. Amara, Y. L. Wang, S. R. Das, C. D. O'Donnell, J. W. Yewdell, K. Subbarao, W. A. Marasco, M. J. Mulligan, R. Compans, R. Ahmed and P. C. Wilson, *J. Exp. Med.*, 2011, **208**, 181–193.
21 F. Hayden, *Clin. Infect. Dis.*, 2009, **48**, S3–S13.
22 G. Vlatakis, L. I. Andersson, R. Muller and K. Mosbach, *Nature*, 1993, **361**, 645–647.
23 H. Q. Shi, W. B. Tsai, M. D. Garrison, S. Ferrari and B. D. Ratner, *Nature*, 1999, **398**, 593–597.
24 G. Wulff, *Angew. Chem., Int. Ed.*, 1995, **34**, 1812–1832.
25 K. Mosbach and O. Ramstrom, *Biotechnology*, 1996, **14**, 163–170.
26 A. L. Hillberg and M. Tabrizian, *IRBM*, 2008, **29**, 89–104.
27 D. R. Kryscio and N. A. Peppas, *Acta Biomater.*, 2012, **8**, 461–473.
28 G. Wulff, A. Sarhan and K. Zabrocki, *Tetrahedron Lett.*, 1973, 4329–4332.
29 G. M. Birnbaumer, P. A. Lieberzeit, L. Richter, R. Schirhagl, M. Milnera, F. L. Dickert, A. Bailey and P. Ertl, *Lab Chip*, 2009, **9**, 3549–3556.
30 L. D. Bolisay, J. N. Culver and P. Kofinas, *Biomaterials*, 2006, **27**, 4165–4168.
31 O. Hayden, P. A. Lieberzeit, D. Blaas and F. L. Dickert, *Adv. Funct. Mater.*, 2006, **16**, 1269–1278.
32 A. Ramanaviciene and A. Ramanavicius, *Biosens. Bioelectron.*, 2004, **20**, 1076–1082.
33 G. Mustafa, M. Hussain, N. Iqbal, F. L. Dickert and P. A. Lieberzeit, *Sens. Actuators, B*, 2012, **162**, 63–67.
34 R. Schirhagl, P. A. Lieberzeit and F. L. Dickert, *Adv. Mater.*, 2010, **22**, 1992.
35 V. P. Torchilin, *Cell. Mol. Life Sci.*, 2004, **61**, 2549–2559.
36 J. Z. Hilt and M. E. Byrne, *Adv. Drug Delivery Rev.*, 2004, **56**, 1599–1620.
37 M. Jenik, R. Schirhagl, C. Schirk, O. Hayden, P. Lieberzeit, D. Blaas, G. Paul and F. L. Dickert, *Anal. Chem.*, 2009, **81**, 5320–5326.
38 J. D. Marty and M. Mauzac, *Adv. Polym. Sci.*, 2005, **172**, 1–35.
39 L. X. Chen, S. F. Xu and J. H. Li, *Chem. Soc. Rev.*, 2011, **40**, 2922–2942.
40 L. I. Andersson, *Bioseparation*, 2001, **10**, 353–364.
41 B. Sellergren, *Anal. Chem.*, 1994, **66**, 1578–1582.
42 S. A. Piletsky, N. W. Turner and P. Laitenberger, *Med. Eng. Phys.*, 2006, **28**, 971–977.
43 F. L. Dickert, O. Hayden, R. Bindeus, K. J. Mann, D. Blaas and E. Waigmann, *Anal. Bioanal. Chem.*, 2004, **378**, 1929–1934.
44 O. Hayden, R. Bindeus, C. Haderspock, K. J. Mann, B. Wirl and F. L. Dickert, *Sens. Actuators, B*, 2003, **91**, 316–319.
45 K. A. Marx, *Biomacromolecules*, 2003, **4**, 1099–1120.
46 J. Matsui, K. Akamatsu, N. Hara, D. Miyoshi, H. Nawafune, K. Tamaki and N. Sugimoto, *Anal. Chem.*, 2005, **77**, 4282–4285.
47 K. Taniwaki, A. Hyakutake, T. Aoki, M. Yoshikawa, M. D. Guiver and G. P. Robertson, *Anal. Chim. Acta*, 2003, **489**, 191–198.
48 Y. Wang, Z. Zhang, V. Jain, J. Yi, S. Mueller, J. Sokolov, Z. Liu, K. Levon, B. Rigas and M. H. Rafailovich, *Sens. Actuators, B*, 2010, **146**, 381–387.
49 D. Cai, L. Ren, H. Zhao, C. Xu, L. Zhang, Y. Yu, H. Wang, Y. Lan, M. F. Roberts, J. H. Chuang, M. J. Naughton, Z. Ren and T. C. Chiles, *Nat. Nanotechnol.*, 2010, **5**, 597–601.

Downloaded by Australian National University on 12 March 2013
Published on 19 February 2013 on http://pubs.rsc.org | doi:10.1039/C3TB00027C

50 A. Merkoci and S. Alegret, *TrAC, Trends Anal. Chem.*, 2002, **21**, 717–725.
51 S. A. Piletsky and A. P. F. Turner, *Electroanalysis*, 2002, **14**, 317–323.
52 C. Malitesta, E. Mazzotta, R. A. Picca, A. Poma, I. Chianella and S. A. Piletsky, *Anal. Bioanal. Chem.*, 2012, **402**, 1827–1846.
53 B. Becker and M. A. Cooper, *J. Mol. Recognit.*, 2011, **24**, 754–787.
54 Y. Amano and Q. Cheng, *Anal. Bioanal. Chem.*, 2005, **381**, 156–164.
55 G. Sauerbrey, *Zeitschrift für Physik*, 1959, **155**, 206–222.
56 K. K. Kanazawa and J. G. Gordon, *Anal. Chem.*, 1985, **57**, 1770–1771.
57 P. Puthavathana, P. Auewarakul, P. C. Charoenying, K. Sangsiriwut, P. Pooruk, K. Boonnak, R. Khanyok, P. Thawachsupa, R. Kijphati and P. Sawanpanyalert, *J. Gen. Virol.*, 2005, **86**, 423–433.
58 A. Thitithanyanont, A. Engering, P. Ekchariyawat, S. Wiboonut, A. Limsalakpetch, K. Yongvanitchit, U. Kum-Arb, W. Kanchongkittiphon, P. Utaisincharoen, S. Sirisinha, P. Puthavathana, M. M. Fukuda and S. Pichyangkul, *J. Immunol.*, 2007, **179**, 5220–5227.
59 A. Seifner, P. Lieberzeit, C. Jungbauer and F. L. Dickert, *Anal. Chim. Acta*, 2009, **651**, 215–219.
60 F. L. Dickert and O. Hayden, *Anal. Chem.*, 2002, **74**, 1302–1306.
61 T. Wangchareansak, C. Sangma, K. Choowongkomon, F. Dickert and P. Lieberzeit, *Anal. Bioanal. Chem.*, 2011, **400**, 2499–2506.
62 M. C. Giocondi, F. Ronzon, M. C. Nicolai, P. Dosset, P. E. Milhiet, M. Chevalier and C. Le Grimellec, *J. Gen. Virol.*, 2010, **91**, 329–338.
63 M. McEvoy, V. Razinkov, Z. Wei, J. R. Casas-Finet, G. I. Tous and M. A. Schenerman, *Biotechnol. Prog.*, 2011, **27**, 547–554.
64 R. W. Ruigrok, A. F. Cremers, W. E. Beyer and F. M. de Ronde-Verloop, *Arch. Virol.*, 1984, **82**, 181–194.
65 C. Baggiani, C. Giovannoli, L. Anfossi, C. Passini, P. Baravalle and G. Giraudi, *J. Am. Chem. Soc.*, 2012, **134**, 1513–1518.
66 H. Jin, G. P. Leser, J. Zhang and R. A. Lamb, *EMBO J.*, 1997, **16**, 1236–1247.

This journal is © The Royal Society of Chemistry 2013